Pre-printed version of the paper published in the journal: Thin-Walled Structures, Vol. 59, pp120-131, 2012

Residual stress study of welded high strength steel thin-walled plate-to-plate joints

Part 2: Numerical modeling

*C. K. Lee, S. P. Chiew and J. Jiang

School of Civil and Environmental Engineering

Nanyang Technological University

50 Nanyang Avenue, Singapore 639798

*Email: ccklee@ntu.edu.sg

ABSTRACT

In the Part 2 of the current study, a sequentially coupled thermal-stress analysis is conducted to model the welding process and the final residual stress distribution of the RQT701 high strength steel thin-walled plate-to-plate welded joints. The accuracy and reliability of the numerical modeling is validated by comparing with the test results. After validating the accuracy of the modeling procedure, a small scale parametric study is carried out to investigate the influences of some key welding parameters on the magnitude and distribution of residual stress.

Key Words: Residual stresses distribution, high strength steel, thin-walled plate-to-plate T and Y-joint, welding parameters

1. INTRODUCTION

Welding, a process by melting the work pieces and adding filler materials to form molten pool, is frequently used in construction of steel structures. In fusion welding, residual stress is induced due to the highly localized, non-uniform and transient heating and the non-linearity of material properties under elevated temperature. The welding process may cause high tensile residual stress in the heat affected zone (HAZ) and lead to fatigue and fracture failures. For thin-walled connections, such effects are more obvious when the base metal is high strength steel (HSS) which often shows a lower ductility when comparing with traditional mild steel. In this case, large residual stresses may affect the fatigue and strength performances of the connection. Therefore, a good estimation of welding residual stress is necessary when HSS is used in structural connections.

During the welding process, the melt metal cools and solidifies as a result of heat conduction in the metal and surface convection and radiation. Therefore, it is necessary to understand the temperature variation with time to evaluate the deformation and residual stress. The heat transfer process in welding plays a key role in the formation of residual stress. During the welding process, the structure is heated unevenly so that high temperature gradient is induced in area chose to the fusion zone. At the same time, the microstructure of steel is changed in the melt zone. Expansion effect in the HAZ is limited by the nearby material so that compressive plastic strain is generated. Eventually, the melt shrinks with restriction from the close-by material in the cooling process and tensile residual stress is generated. On the whole, welding is a complicate coupled thermo-mechanical process and consequently numerical studies are deemed to be necessary in order to understand the influences of different key welding parameters on the distribution of the final residual stress.

To accurate predict the welding residual stress field, a reliable heat model is necessary to describe and analysis the process of heat transfer in the welding procedure. Sheng and Chen [1] incorporated a fluid-flow model in the thermo-mechanical analysis. Goldak et al. [2] suggested that the best way to create reliable heat input model is to measure the temperature field experimentally and then adjust the heat input until good agreements are obtained. It has been shown [3] that when the heat source has been calibrated, the approach used in computational welding mechanic is sufficient to produce good residual stress prediction. Masubuchi [4] gave a summary of several heat input models for residual stress simulation. Hibbitt and Marcel [5] used surface heat input and an impulse equation to describe the heat contributed by the addition of weld filler. Many researchers [6-11] explored the residual stress modeling techniques for different kinds of welding cases. In addition, several reviews were conducted [12-19] on the mechanical effects of welding. In the process of welding simulation, some simplifications or assumptions are frequently needed to reduce the computational cost. The lumped technique, in which two or more welding passes are combined into one block during the numerical modeling, is one of the most commonly used techniques employed to obtain a reasonable trade-off between the accuracy and computational cost. To validate the acceptability of this technique, some researchers investigated the effects of different lumping schemes [20-24].

Since testing is costly, time-consuming and limited in obtaining data, finite element modeling is widely used in studying the residual stress formation and distribution caused by welding. Therefore, in this paper a carefully selected sequentially coupled thermal-mechanical analysis procedure was employed for residual stress analysis for the HSS plate-to-plate joints that were studied experimentally earlier [25]. Validation of the analysis procedure will be conducted by comparing the numerical results with the experimental results. After validating the accuracy of the modeling procedure, a small scale parametric study will be carried out to investigate the

influences of some key welding parameters such as the boundary conditions, the preheating temperature, the numbers of welding pass, the welding speed and the welding sequence on the magnitude and distribution of residual stress.

2. MODELING PROCEDURE AND TECHNIQUE

2.1. Overview

In this paper, the finite element modeling package ABAQUS [26] was used to model the welding process. A sequentially coupled thermal-stress analysis was conducted by assuming that the stress solutions are dependent on the temperature fields while there is no inverse dependency. Sequentially coupled thermal-stress analysis was performed by first solving the non-linear transient heat transfer problem. The time-dependent temperature data were then fed into the stress analysis model as a predefined field (Fig. 1). During the thermal analysis, it was assumed that the stress generated in welding has negligible influence on the temperature field. Furthermore, the heat convection and radiation effects were both considered in the modeling. Table 1 gives a summary for the sequentially-coupled thermal-stress analysis procedure. Since in the experimental study [25], it was found that the residual stress in the middle cross section of plate (the cross section on which the points B, B1, B2 and B3 are located, Fig. 7 of reference [25]) is much higher than that at the two ends, in order to reduce the computational cost of the numerical modeling, 2D plane strain models were created to study the residual stress variation at the middle cross sections of the thin-walled plate-to-plate joints [27, 28]. The 2D finite element mesh used in the analysis is shown in Fig. 2. Note that in order to optimize the efficiency of the numerical model, larger elements were used to discretize the base plate while refined elements were used to model the weld filler.

2.2 The lumped technique

One popular approach to simplify the modeling procedure and to reduce the computational cost needed is the lumped technique [20-24]. When this technique is employed, two or more weld passes are condensed into one weld block or lump. Hence, rather than analyzing the temperature variation and stress formation for every weld pass, numerical simulations will only be needed for a few lumps. By using different lumping schemes, the coarsest and the most accurate solutions could be obtained by using just one lump and as many lumps as the actual weld passes, respectively. In practice, a reasonable number of lumps should be selected in order to balance the accuracy and the computational cost. In the experimental study [25], it was recorded that 9 to 22 weld passes were employed in the welding of the plate-to-plate joints. In the numerical study, it was found that they could be lumped into four welding blocks to reduce the computational cost of the modeling procedure while maintaining the accuracy of the modeling results.

2.3 The weld filler addition (birth and death) technique

The element 'birth and death' technique was used for simulation of the addition of the weld filler materials [26]. At the beginning of the modeling, all elements corresponding to the weld filler were deactivated by setting their stiffness to zero. As the welding was proceeding on, the deactivated elements would be re-activated by setting them with the appropriate material properties. Such "birth and death" technique simplifies the modeling procedure as only a single finite element mesh is needed. However, this technique may introduce problems into the stress analysis phase since large displacements would be induced by the heating and cooling process especially near those regions where many "death" elements are located. The boundary between old and newly added elements may be strongly distorted. Furthermore, attempts to fit the fresh filler into the deformed model will cause redistribution of the residual stresses inherited from

previous passes. To eliminate such adverse effect, an auxiliary step was performed whenever after a new set of elements were added. In this step, a lower stiffness was assumed for the newly added elements by multiplying a reduction factor of 0.35 to the true value and plastic strains were removed from the model. Each auxiliary step is lasted for 1.0s and this time was excluded from the actual heat transfer and stress analyses since this step is employed to transit the deformed geometry from the previous pass to the next addition of weld filler. As shown in Fig. 2(a), the model of the joint was first created by including all the elements for the base plates and weld filler. At the beginning of the analyses, all weld filler elements were first deactivated. As the welding started, the first lump of weld filler was activated at 0.001s (Fig. 2b). The second and the other lumps were then activated sequentially (Figs. 2c-2e).

2.4 Heat transfer analysis

The heat transfer analysis was conducted based on the thermal energy balance principle, which could be stated mathematically as:

$$\int \delta_\theta \rho \dot{E} dV - \int \frac{d\delta_\theta}{dx} \cdot q dV = \int \delta_\theta \rho dS + \int \delta_\theta r dV \quad (1)$$

In the Eqn. (1), q is heat flux per unit of current area crossing surface S from the environment into the body. r is the heat flux per unit volume generated within the body. ρ is the material mass density. $\dot{E}$ is the internal energy per unit mass and δ_θ is an arbitrary variation of the temperature field.

In the thermal analysis, transient non-linear analysis was conducted for the 2D model to determine the temperature history throughout the heating and cooling process during the welding. The heat flux q was modeled by relating it with the welding speed v, which is linked to the arc voltage U (26V) and the arc current I (170A). In the numerical model, a reasonable heating

duration Δt accounting for the effect of moving heat source on the target cross section should be determined. This was achieved by adjusting the amplitude of the heat source density curve in such a way that melting temperature (1300-1400°C) was attained in the molten zone and a maximum temperature of 500-600°C was attained in the HAZ. The distributed heat flux is defined by the equation:

$$q = \frac{\eta UI}{l_w h_w v} \tag{2}$$

In Eqn. (2), η=0.8 is the arc efficiency factor, l_w is the width of each lump, h_w is the height of each lump.

A typical heat transfer analysis contains thermal material nonlinearities and boundary nonlinearities. Material nonlinearities include the thermal conductivity k and the specific heat c which are functions of temperature [29]. Boundary nonlinearities include convection and radiation effects were both considered in the modeling of the heat loss on the surface of the joint. The convection coefficient h was defined as 15W/ m^{2}K and the emissivity ε was set as 0.2. In all numerical models, the variations of thermal conductivity, specific heat and thermal expansion coefficients with temperature for the RQT701 HSS plate were obtained from the Eurocode 3 Part 1-2 [30] and are shown in Fig. 3.

In order to evaluate the effect different key welding parameters on the cooling rate of the joints, the *average cooling rate* K_t at a given point of the joint was calculated. For a selected point of the joint, K_t is defined as the temperature gradient between the time when the maximum temperature is attained to the time when the temperature at that point is dropped back to 100°C and can be computed as:

$$K_t = \frac{T_{max} - 100°C}{t_{max} - t_{100}} \tag{3}$$

In Eqn. (3), T_{max}> 100°C is the maximum temperature reached during the welding process. t_{max} is the time when the maximum temperature is attained. t_{100} is the time when the temperature of the point is dropped back to 100°C.

2.5 Mechanical analysis

In the mechanical analysis, the temperature history obtained from the thermal analysis was input as a thermal loading into the stress analysis model. To make the process of feeding temperature field into the stress analysis model an easy task to handle, a compatible mesh with the same meshing topology and element numbering was used. However, it should be noticed that in order to obtain accurate stress analysis results, the CPE8R element which is an 8-node bi-quadratic plane strain element with reduced integration, was employed during stress analysis while the 4-node linear element DC2D4 was employed for the thermal analysis to obtain stable results. Table 1 summarizes the detailed information for the analysis models.

While the temperature dependent thermal properties of the RQT701 HSS plate were obtained from the Eurocode 3 Part 1-2 [30], the mechanical properties including the Young's modulus E, the yield strength f_y and the ultimate strength f_u were obtained by performing coupon tests at normal and elevated temperature as recommended by the relevant testing standard [31]. Fig. 4 shows the variations of these mechanical properties as functions of temperature and their comparisons with the recommended values from the Eurocode 3. Note that as the Eurocode 3 is mainly applicable to the normal mild steel, there are noticeable differences between the Eurocode 3 curves and the test curves especially for the E value for the HSS plates used.

3 MODEL VALIDATION AND RESULTS

3.1 Model validation

In this section, in order to validate the model accuracy, the numerical modeling results obtained from the sequentially coupled thermal-mechanical analysis are compared with the experimental data obtained. In the experimental study [25], twelve joints were fabricated (without brace plate cutting) for residual stress measurement. Therefore, twelve numerical models were created corresponding to the joints tested. Table 2 lists the detailed results at the measurement points where experiment results are available. After comparing with the experimental results obtained, in general, it is found that the numerical model adopted could able to predict the residual stress distributions of all test joints with reasonable accuracy.

Figs. 5 and 6 compare the results obtained from the six 90° joints tested. From Fig. 5, it can be seen that for joints with preheating, at the 5mm measurement point the differences between the numerical and measured transverse residual stress values are reasonable (31.0MPa, 39.1MPa and 1.0MPa for 8mm, 12mm and 16mm specimens respectively). It is interested to note that in the numerical study, the residual stress *range* for joints with different plate thicknesses (8mm to 16mm) is smaller than the corresponding range obtained from experimental measurements. This phenomenon may be explained by the fact that during actual welding, imperfectness such as breaking-off, insufficient weldment and geometrical error often occurs. Nevertheless, the stress differences between the modeling and testing are smaller than 50MPa at all the positions. Similarly, as shown in Fig. 6, the modeling results are well coincidence with testing results for 90° joints welding at ambient temperature, especially at the 5mm point.

Figs. 7 and 8 provide similar comparisons between the model and test results for the six 135° joints tested. For preheating joints at the 5mm measurement point, the differences between the numerical and measured results are again very reasonable (16.7MPa, 38.6MPa and 11.1MPa for

8mm, 12mm and 16mm joints respectively). In Fig. 8, similar results could again be observed except for the 16mm joint with a difference of 64.2MPa.

3.2 Discussions on the modeling results

3.2.1 Temperature distribution history

To understand the temperature variations and residual stresses formation process during the welding, the temperature distributions near the weld region are carefully studied. The typical results from the joint with θ=135°, t_1=12mm which was welded at ambient temperature is taken as an example in this section for discussion. Fig. 9 shows the temperature distribution history of this joint near the welding region (area enclosed by the dash lines in Fig. 2(a)). Fig. 9(a) shows the temperature distribution at 1.0s after the welding started. At that moment, as all other weld lumps were still deactivated, heat energy was mainly propagated only to a small localized area of near the chord and the brace plate intersection. Fig. 9(b), 9(c), 9(d) show the temperature distributions at the moments 1 second after the 2^{nd}, 3^{rd} and 4^{th} lumps were added, respectively. From Fig. 9(a) to 9(d), it can be seen that as the welding proceeded on, more heat was transferred from the center of heat source (the activated lumps) to the ends of the plates. When the propagation time was 300s (Fig. 9(e), a transient moment during the cooling period), the weld part and the regions in the chord plate which is directly beneath the weld attained their highest temperature when comparing with other parts of the connection. When the propagation time was 2500s, shown in Fig. 9(f), the steady state temperature distribution was reached for the whole joint and the final residual stress distribution was formed.

3.2.2 Residual stress distributions

Fig. 10(a) and Fig. 10(b) show the residual stress at the final steady stage for a joint (θ=135° and t_1=12mm) weld at 100°C preheating and ambient temperature, respectively. From Fig. 10, it can be seen that preheating can effectively reduce final tensile residual stress induced, especially at region near the weld toe and at the bottom part of the chord plate. In fact, detailed analysis found that at the final state, the transverse residual stresses at the weld toe are 316.5MPa and 408.7MPa respectively for joints with and without preheating.

Figs. 11 and 12 respectively show the development history for the transverse residual stress at different propagation times for the same joints with and without preheating. From these two figures, it can be seen that when the propagation time is 57.7s (the moment when the 2nd lump is about to add), the residual stress at the weld toe was increased to 330MPa for the joint welded at ambient temperature while the residual stress at the weld toe is 148.6MPa for the preheated joint. Therefore, preheating can significantly reduce the magnitude of the residual stress *before* the 2nd lump of weld was added. From Fig. 12, it can be seen that for the joint welded at ambient temperature, the residual stress at the weld toe was mainly formed (>300MPa) during the time interval between the welding started and the moment when the 2nd lump of weld was added and there was only a relative small increase (≈100MPa) in the magnitude of the residual stress during the addition of remaining lumps. For the joint welded with preheating, the development of residual stress was more evenly spread among the welding process. It could be seen that the contributions from the additions of the 1st lump (≈150MPa) and the 2nd lumps (≈50MPa) as well the final cooling step (≈80MPa) are all significant. Figs. 11 and 12 also show that the residual stress variation was highest in the region within 10mm from the weld toe and this reconfirmed

the earlier observations of the highly localized property of heating and residual stress formation process during welding.

Fig. 13 shows the average cooling rate K_t (Eqn. 3) for the two joints. It can be seen that the average cooling rate for preheated joint is obviously lower than the joint without preheating, especially at region within 20mm from the weld toe and such result is consistent with both the measured [25] numerical results (Figs. 11 and 12) and could explain why preheating could effectively reduce the magnitude of residual stress near the weld toe.

4 PARAMETRIC STUDY

After validating the accuracy of the numerical modeling procedure, a small scale of parametric study was be carried out. Twenty three models were created to investigate the effects of (i) the mechanical boundary conditions, (ii) the preheating temperature, (iii) the numbers of weld lump, (iv) the welding speed and (v) the welding sequence on the distributions of final residual stress and the average cooling rate. In order to keep the number of models within a manageable limit, each parameter was analysed separately by keeping other parameters constant and only the joint with θ=135° and t_1=12mm was studied. Table 3 summaries the details of the 23 models created. Figs. 14, 15 and 16 respectively show the three mechanical boundary conditions, the four lumping schemes and the four welding sequences employed in the parametric study. It should be noted the actual welding speed adopted during fabrication is 2.6mm/s and the welding sequence shown in *case a* of Fig. 16 is corresponding to the actual welding sequence employed during the fabrication of the joint [25].

4.1 Effect of boundary condition

Fig. 17 shows the relationships between the transverse residual stress and the distance from the weld toe when different boundary conditions were applied. Three different boundary conditions correspondiong the fixed, pinned and simply supports were considered. From Fig. 17, it can be seen that there exists a moderate difference (42.6 MPa) at the weld toe between the fixed and the pinned support boundary conditions. However, the corresponding difference between the pinned and simply support cases was smaller (10.7MPa). Furthermore, by comparing the modeling results with test results, it could be concluded that the actual support condition should be somewhere between the pinned and fixed supports. However, it should be noted that while the pin or simply support can lead to lower residual stress, the angular distroration and deformation of the joint would be more serious than the fixed supports.

4.2 Effect of preheating temperature

Fig. 18 shows the relationship between the transverse residual stress and the distance from the weld toe when different preheating temperatures were applied. The preheating areas are within 30mm from the welding connection (Fig. 3 of reference [25]). During modeling, the preheating effect was added as a predefined constant temperature field in the model before the first weld lump was added in. From Fig. 18, it can be seen that the residual stress value at the weld toe is sensitive to the preheating temperature. When the preheating temperature was increased from 75°C to 300°C, the transverse residual stress was dropped from 241.2MPa to 66.2MPa. Note that when the joint is welded in ambient temperature, the transverse residual stress at the weld toe is 293.3MPa. From Fig. 18, it can be again concluded that preheating can effectively relieve residual stress near the weld toe. Furthermore, Fig. 18 also reconfirms that such reduction effect will not be significant for region located beyond 15mm from the weld toe.

Fig. 19 shows the variation of the average cooling rate when different preheating temperatures were applied. When comparing Fig. 18 with Fig. 19, a similar trend can be observed that at the weld toe, the average cooling rate is the largest when the joint was fabricated at the ambient temperature and the average cooling rate was reduced as the preheated temperature was increased. In addition, the average cool rate dropped quickly with the increase of the distance from the weld toe when the perheating temperature is lower than 150°C.

4.3 Effect of using different number of weld lumps

In order to find out the influence of the numbers of weld lump used during modeling to the predicted value of residual stress, the residual stress distributions obtained for four different lumping schemes with 2 to 16 lumps were computed and the results are shown in Fig. 20. From Fig. 20, it can be concluded that the predicted residual stress at the weld toe was reduced as the numbers of weld lump employed was increased. For the joints studied, the residual stress at the weld toe was decreased from 336.7MPa to 263.6MPa as the numbers of weld lump was increased from 2 to 16. In particalar, when the numbers of lumps was increased from 2 to 8, the magnitude of residual stress at the weld toes was reduced significantly (74MPa) while only a small drop (8.2MPa) occurred when the numbers of lumps was increased from 8 to 16. Based on the above results, it is suggested that in practice, 4 weld lumps should be applied to plate-to-plate HSS joint modeling in order to obtain conversative residual stress prediction with reasonable computational resource needed.

Fig. 21 shows the varation of the average cooling rate when different lumping schemes were used. Similar to Fig. 20, again it can bee seen that the avarage cooling rate dropped as more weld lumps were employed during the modeling.

4.4 Effect of welding speed

It should be mentioned that during the parametric study of welding speed, it was assumed that the same welding equipment with the same setting were used when the welding speed was varied. Hence, both the current and voltage applied were kept constant. From Eqn. 2 (Section 2.4), this implies that as the welding speed is increased, the value of heat flux will be decreased. Together with the obvious fact that a higher welding speed implies a shorter heating time of the section under consideration, it can be concluded that when a higher welding speed is applied, *less* heat input per unit length will be passed into the joint and it is likely to decrease the magnitude of the residual stress. Fig. 22 shows that the influence of welding speed on the transverse residual stress distribution. As expected, the residual stress decreased as the welding speeding increased. In addition, Fig. 22 shows the residual stress at the weld toe was sensitive to welding speed when it was slower than 2.6mm/s. When the weld speed was 2.0mm/s, 2.2mm/s and 2.4mm/s, the correspondingly residual stresses at the weld toe were 351.7MPa, 341.3MPa and 318.7MPa. When the weld speed was increased to 2.8mm/s and 3.0mm/s, the stress decreased to 242.6MPa and 187.6MPa, respectively. Fig. 23 shows the variation of the average cooling rate when different welding speeds were applied in the modeling. Again, similar to Fig. 22, the average cooling rate near the weld toe decreased as the welding speed increased.

4.5 Effect of welding sequence

Four different welding sequences, as shown in Fig. 16, were studied to evaluate their influences on the residual stress. Figs. 24 and 25 show respectively the variation of the transverse residual stress and the corresponding average cooling rates when different welding sequences were applied. From Figs. 24 and 25, it can be concluded that welding sequences *a* produced the lowest residual stress at the weld toe. This observation could be explained by the fact that during a

multi-pass welding, the first welding pass in fact provides some preheating effects for the following welding process. When sequence *a* is applied, the weld toe near the brace and chord plates intersection was heated up more uniformly after the first weld pass was added. Sequentally, after all weld fillers were added, the cooling rate at the weld toe becomes lower and this leads to lower residual stress.

Finally, based on parametric study results presented in this section, it could be concluded that the boundary condition, the preheating temperature, the welding speed, the welding sequence and the numbers of weld lump all have noticeable impacts on the mangnitude of the residual stress at the weld toe of the HSS plate-to-plate joints. Furthermore, increasing of preheating temperature and the welding speed could reduce the magnitude of residual stress.

5. CONCLUSIONS

The paper has presented a sequentially coupled thermal-stress analysis procedure for the welding process modeling of high stress steel (HSS) thin-walled plate-to-plate welded joints. The element 'birth and death' and the lumping are employed in the addition of filler during the welding process. It is found that the sequential coupled thermo-mechanical employed could produce reasonably accuracy predictions of the final residual stress distributions of the joints.

A small scale parametric study has been carried out to evaluate the influence of the mechanical boundary conditions, the preheating temperature, the numbers of weld lump, the welding speed and the welding sequence on the distributions of the final residual stress. It is found that the fixed supported conditions could lead to a higher transverse residual stress at weld toe. For preheating treatment, it is shown that it could reduce the magnitude of the residual stress at the weld toe. In particular, for the HSS thin plates used in this study, such effect is more obvious when the

preheating temperature exceeds 150°C. For the effects of lumping scheme adopted, it is shown that increasing the number of weld lumps in the numerical model tends to reduce the residual stress predicted. Finally, study on the welding speed and welding sequence show that the residual stress near the weld toe could be lowered by increasing the welding speed and adopting a welding sequence which could heat up the intersection between the brace plate and the chord plate more uniformly.

Acknowledgment: The financial support of the Regency Steel Asia to the authors is gratefully acknowledged. The helps from the Yongnam Pte Ltd. for the fabrication of the test specimens are also appreciated.

References:

[1] Sheng IC and Chen Y (1992). Modeling welding by surface heating, J. Engineering Materials and Technology, vol. 114, pp. 439-449.

[2] Goldak J, Chakravarti A, and Bibby M (1983). A new finite element model for welding heat sources, Metallurgical Transactions B, Vol, 15B, June.

[3] Lindgren LE. Computational welding mechanics. Thermomechanical and microstructural simulations.2007: Woodhead Publishing.

[4] Masubuchi K. Analysis of welded structures, Pergamon Press, 1980.

[5] Hibbitt HD and Marcal PV (1973). A Numerical Thermo-Mechanical Model for the Welding and Subsequent Loading of a Fabricated Structure, Computers & Structures, vol. 3, pp. 1145-1174.

[6] Shahram Sarkani, Vesselin Tritchkov and George Michaelov. (2000). An efficient approach for computing residual stresses in welded joints, Finite Elements in Analysis and Design, vol. 35, pp. 247-268.

[7] Gery D, Long H, and Maropoulos P (2005). Effects of welding input and heat source distribution on temperature variations in butt joint welding, Journal of Materials Processing Technology, vol. 167, pp. 393-401.

[8] Kyong-Ho Chang and Chin-Hyung Lee (2009). Finite element analysis of the residual stresses in T-joint fillet welds made of similar and dissimilar steels, The International Journal of Advanced Manufacturing Technology, vol. 41, pp. 250-258.

[9] Chin-Hyung Lee and Kyong-Ho Chang (2007). Numerical analysis of residual stresses in welds of similar or dissimilar steel weldments under superimposed tensile loads, Computational Materials Sciences, vol. 40, pp. 548-556.

[10] Vakili-Tahami F, Daei-Sorkhabi AH, Saeimi-SMA, Homayounfar A (2009). 3D finite element analysis in butt-welded plates with modeling of the electrode-movement, Journal of Zhejiang University Science A, vol. 10, pp. 37-43.

[11] Mok DHB and Pick RJ (1990). Finite element study of residual stresses in a plate T joint fatigue specimen, IMechE Part C: Journal of Mechanical Engineering Science, vol. 204, pp. 127-134.

[12] Karlsson L. Thermal stresses in welding, Thermal Stresses Vol (I), Elsevier Science Publishers, 1986.

[13] Smith SD. A review of weld modeling for the prediction of residual stresses and distortions due to fusion welding, Proceeding of 5th International Conference on Computer Technology in Welding, 1992.

[14] Radaj R. Heat effects of welding, Springer-Verlag, 1992.

[15] Radaj R. Finite element analysis of welding residual stresses, Proceeding of 2nd International Conference on Residual Stress, 1988.

[16] Lindgren LE. (2001) Finite element modeling and simulation of welding Part 1: Increased complexity, Journal of thermal stresses, vol. 24, pp. 141-192.

[17] Lindgren LE (2001). Finite element modeling and simulation of welding Part 2: Improved material modeling, Journal of thermal stresses, vol. 24, pp. 195-231.

[18] Lindgren LE (2001). Finite element modeling and simulation of welding Part 3: Efficiency and integration, Journal of thermal stresses, vol. 24, pp. 305-334.

[19] Lindgren LE. (2006). Numerical modelling of welding. Computer Methods in Applied Mechanics and Engineering, 195, 6710-6736.

[20] Ueda Y and Nakacho K. (1982). Simplifying methods for analysis of transient and residual stresses and deformations due to multipass welding, Transactions of Joining and welding Research Institute, Osaka University, vol. 11, pp. 95-103.

[21] Rybicki EF, Schmueser DW, Stonesifer RB, Groom JJ and Mishler HW (1978). A finite element model for residual stresses and deflections in girth-butt welded pipes, Journal of Pressure Vessel Technology, vol. 100, pp. 256-262.

[22] Rybicki EF and Stonesifer RB (1979). Computation of residual stresses due to multipass welds in piping systems, Journal of Pressure Vessel Technology, vol. 101, pp. 149-154.

[23] Free JA and Porter Goff RFD (1989). Predicting residual stresses in multi-pass weldments with the finite element method, Computers & Structures, vol. 32, pp. 365-378.

[24] Hong JK, Tsai CL and Dong P (1998). Assessment of numerical procedures for residual stress analysis of multipass welds, Welding Journal , vol. 77, pp. 372-382.

[25] Lee CK, Chiew SP, Jiang Jin, Residual stress study of wielded high strength steel plate-to-plate joints, Part 1: Experimental study, Accepted for publication by the Thin-Walled Structures.

[26] ABAQUS User Manual, version 6.9. Hobbit, Karlsson & Sorensen Inc., USA.

[27] Berglund, D. and H. Runnemalm. Comparison of deformation pattern and residual stresses in finite element models of a TIG-welded stainless steel plate. in 6th International Conference on Trends in Welding Research. 2002. Pine Mountain, Georgia: ASM International.

[28] Goldak, J., et al. Computational weld mechanics. in AGARD Workshop - Structures and Materials 61st Panel meeting. 1985. Oberammergau, Germany.

[29] Lindgren LE, Runnemalm H and Näsström MO (1999). Numerical and experimental investigation of multipass welding of a thick plate, International Journal for Numerical Methods in Engineering, vol. 44, pp. 1301-1316.

[30] Eurocode 3. Design of steel structures Part 1-2: General rules — Structural fire design. 2005.

[31] BS-EN 10002-5, Tensile testing of metallic materials Part 5: Method of test at elevated temperatures, British Standard Institute (BSI), 1992.

Nomenclature

A	Cross-sectional area of a weld lump
c	Specific heat
$\dot{E}_{\text{gen}}$	Heating rate generated from a weld lump
E	Young's modulus of steel
f_{y}	Yield stress of steel
h	Convection coefficient
h_{w}	Height of a weld lump
I	Arc current
K_t	Average cooling rate
k	Material conductivity
l_{w}	Width of a weld lump
q	Heat flux from outside into the body
q_{c}	Net rate of convection heat transfer
q_{r}	Net rate of radiation heat transfer
r	Heat flux generated in the body
T	Temperature
T_0	The ambient temperature (30°C)
T_b	Benchmark temperature
t	Heat propagation time (time after the welding started)
t_1	The thickness of the base steel plate
U	Arc voltage of welding
A	Thermal expansion coefficient
E	Emissivity coefficient
σ_{B}	The Stefan-Boltzmann coefficient
P	Material mass density
ν	Poisson's ratio
θ	Joint angle
δ_θ	An arbitrary variation of the temperature field
Δt	Time increment in the modeling
Δl	Distance between nodes
$[C]$	Heat capacitance matrix
$[K]$	Thermal conductivity matrix
$\{Q\}$	External flux vector
$\{T\}$	Temperature field
$\{\sigma\}$	Stress field
HSS	High strength steel
HAZ	Heat affected zone

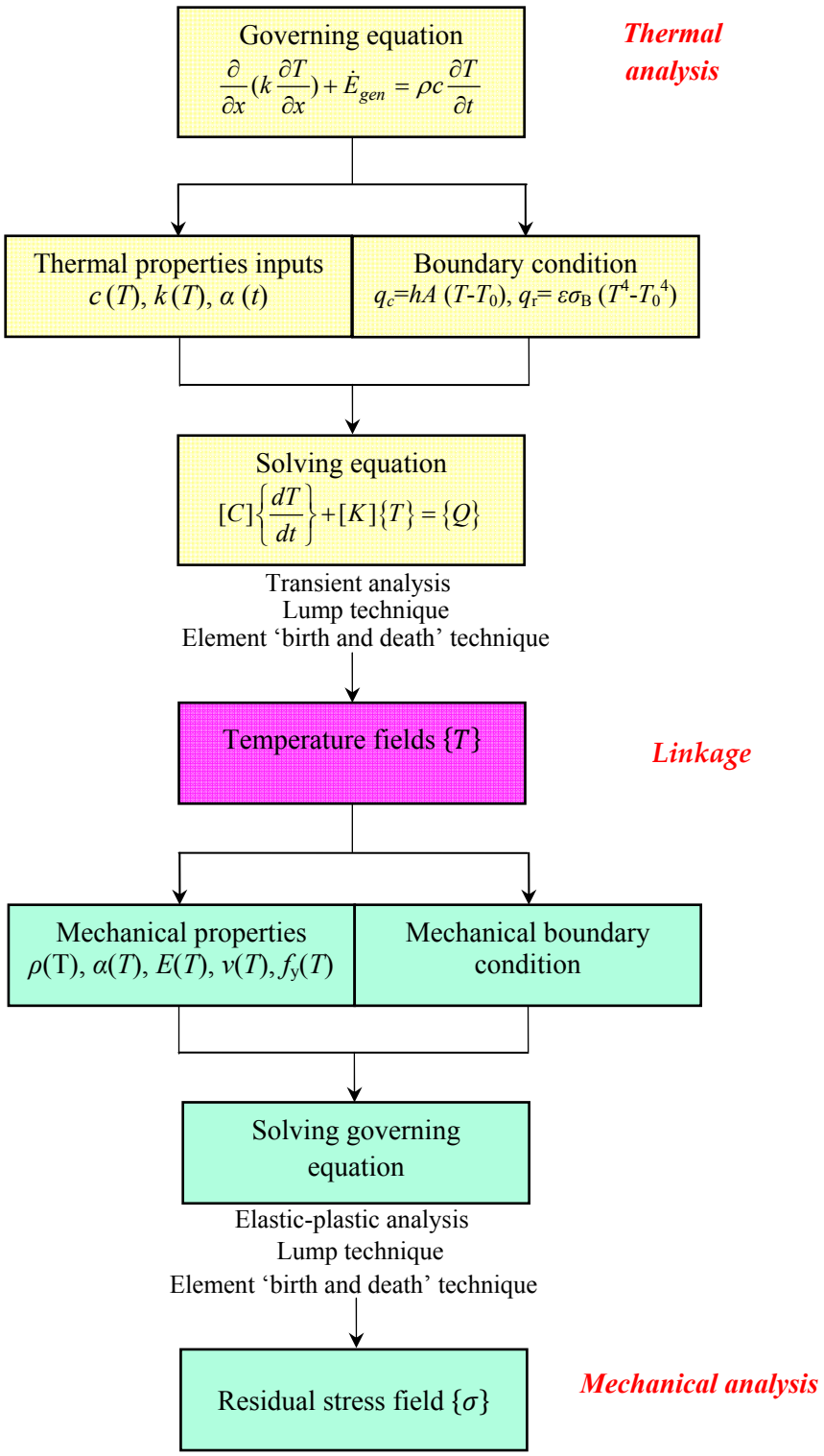

Fig. 1 The overall flow chart of the numerical modeling of the welding procedure

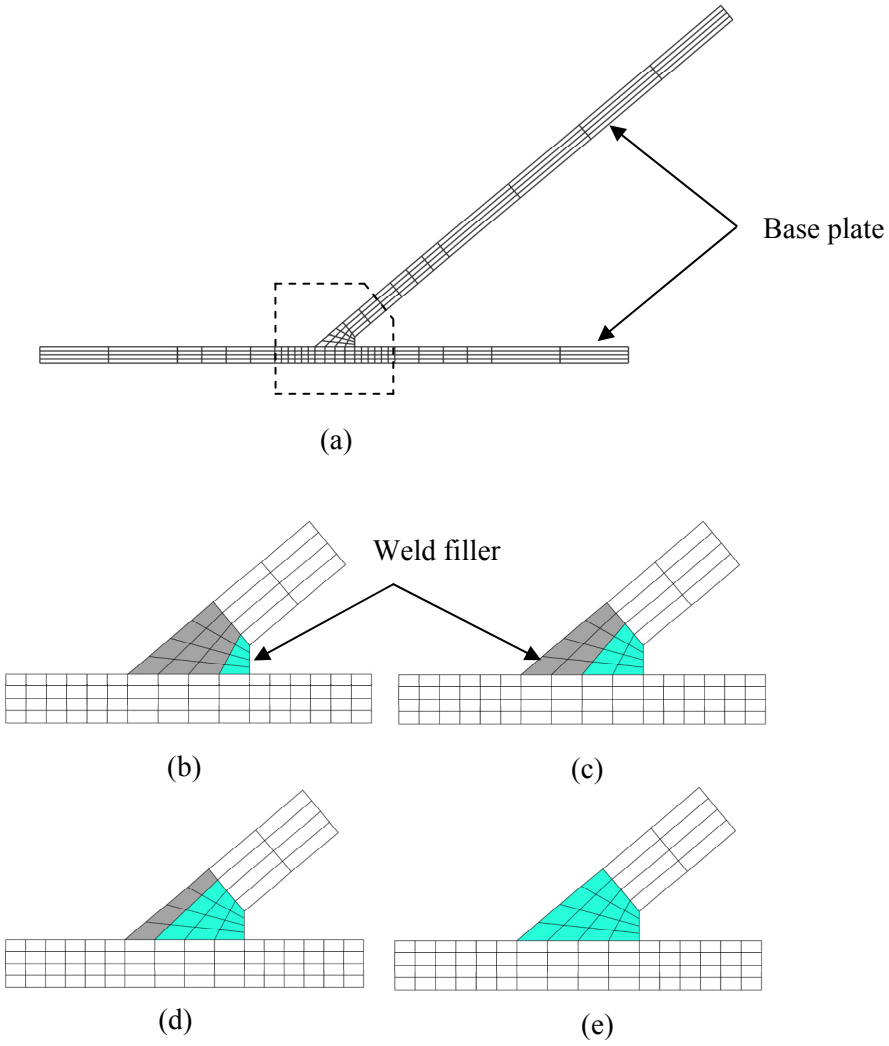

Fig. 2 Finite element discretization of the plate-to-plate joint
Blue elements: activated, Gray elements: deactivated

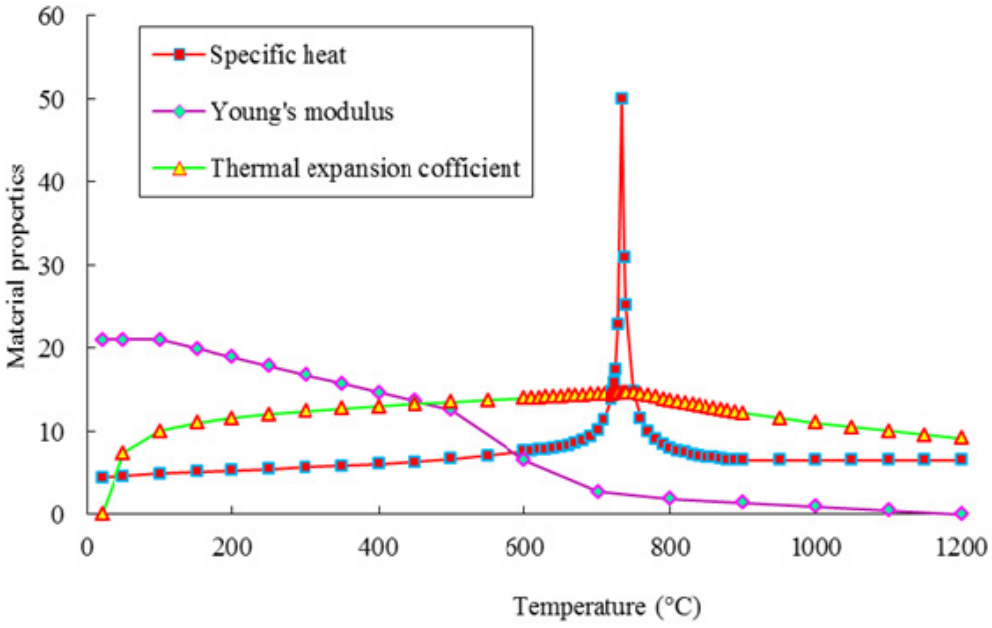

Symbol	Material properties	Unit
c	Specific heat	10^2J/(K.Kg)
k	Thermal conductivity	W/(K.m^2)
α	Thermal expansion coefficient	10^{-6}/K

Fig. 3 The thermal material properties of steel based on the Eurcode 3

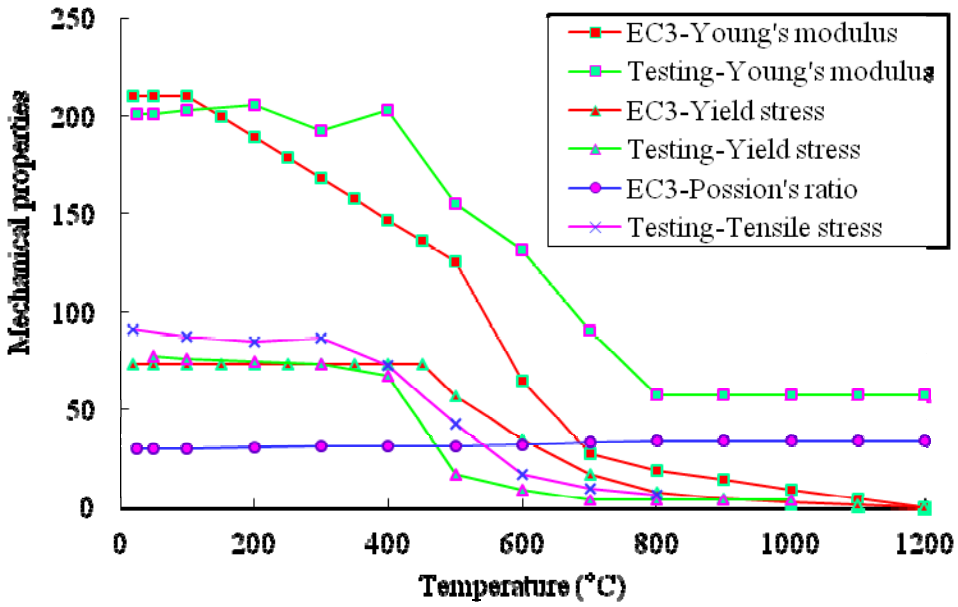

Symbol	Material properties	Unit
E-EC3	Young's modulus from EC3	GPa
E-Testing	Young's modulus from coupon test	GPa
f_y-EC3	Yield stress from EC3	(×10)MPa
f_y-Testing	Yield stress from coupon test	(×10)MPa
v- EC3	Poisson's ratio from EC3	($\times 10^{-2}$)
f_u-Testing	Tensile stress from coupon test	(×10)MPa

Fig. 4 Comparison of mechanical material properties of high strength steel between coupon test results and suggested values from the Eurocode 3

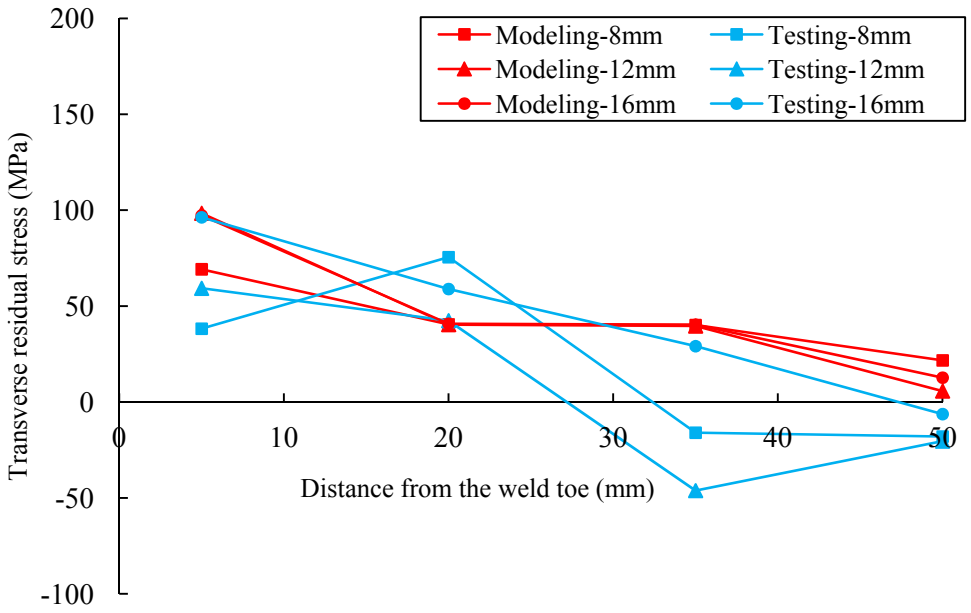

Fig. 5 Comparison of modeling and test results for θ=90° joints with preheating

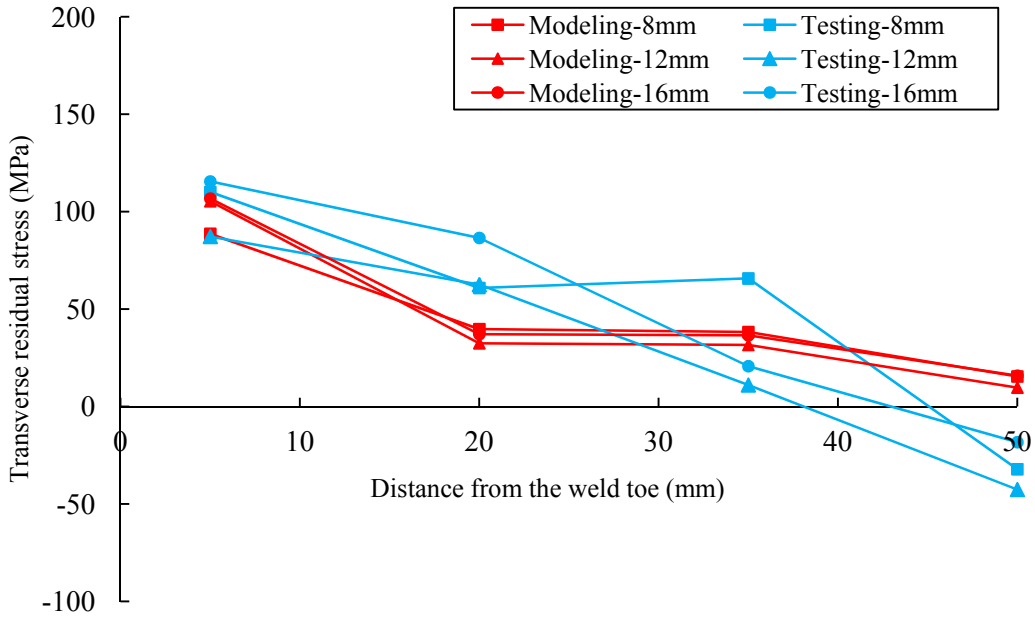

Fig. 6 Comparison of modeling and test results for θ=90° joints welded at ambient temperature

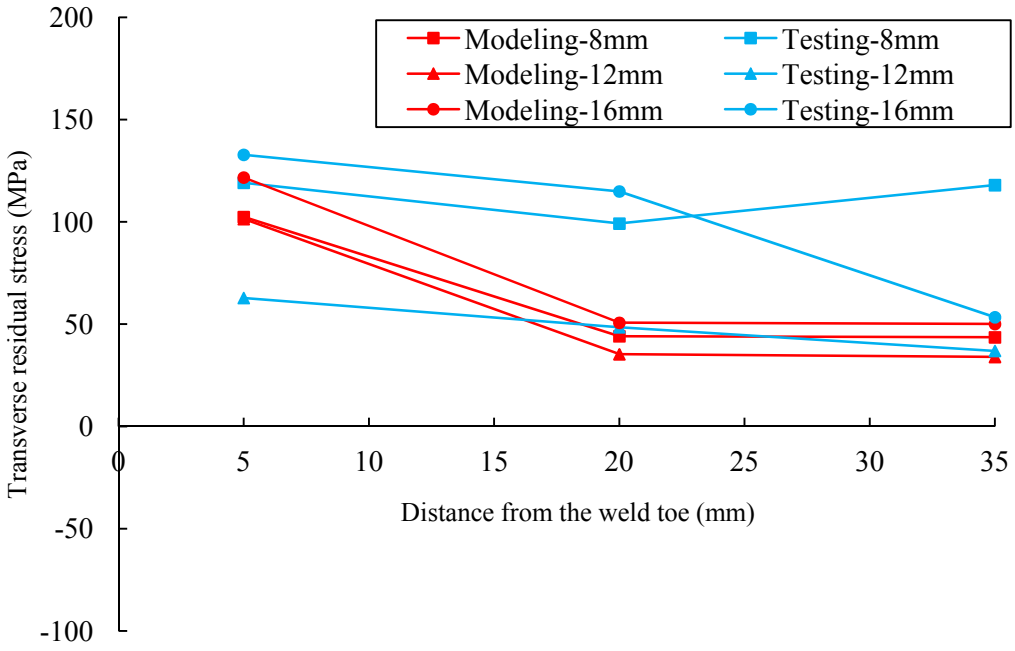

Fig. 7 Comparison of modeling and test results for θ=135° joints with preheating

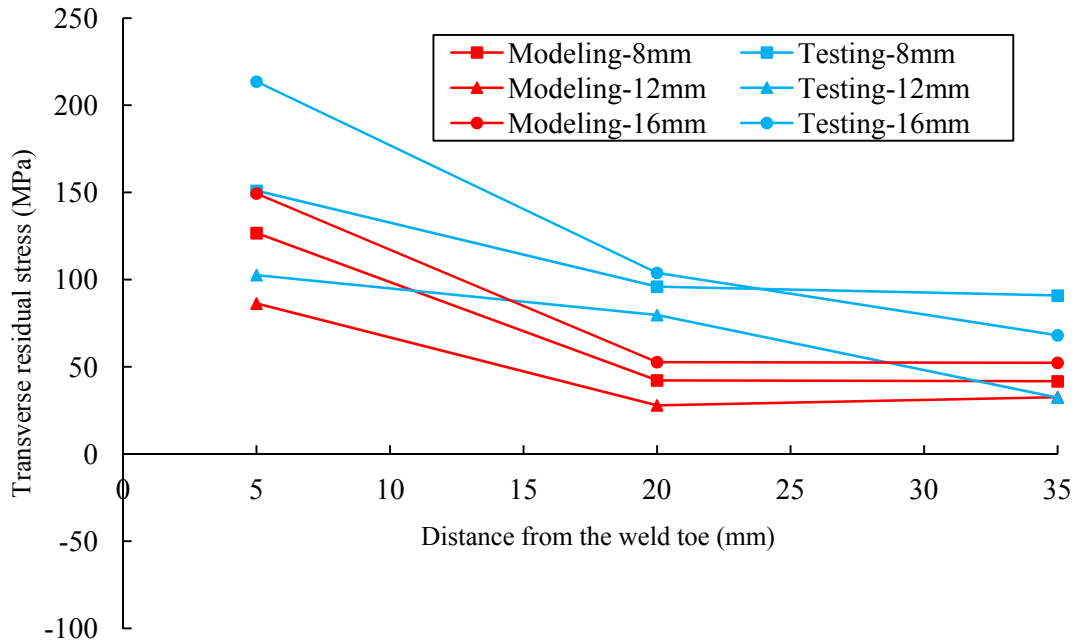

Fig. 8 Comparison of modeling and test results for θ=135° joints welded at ambient temperature

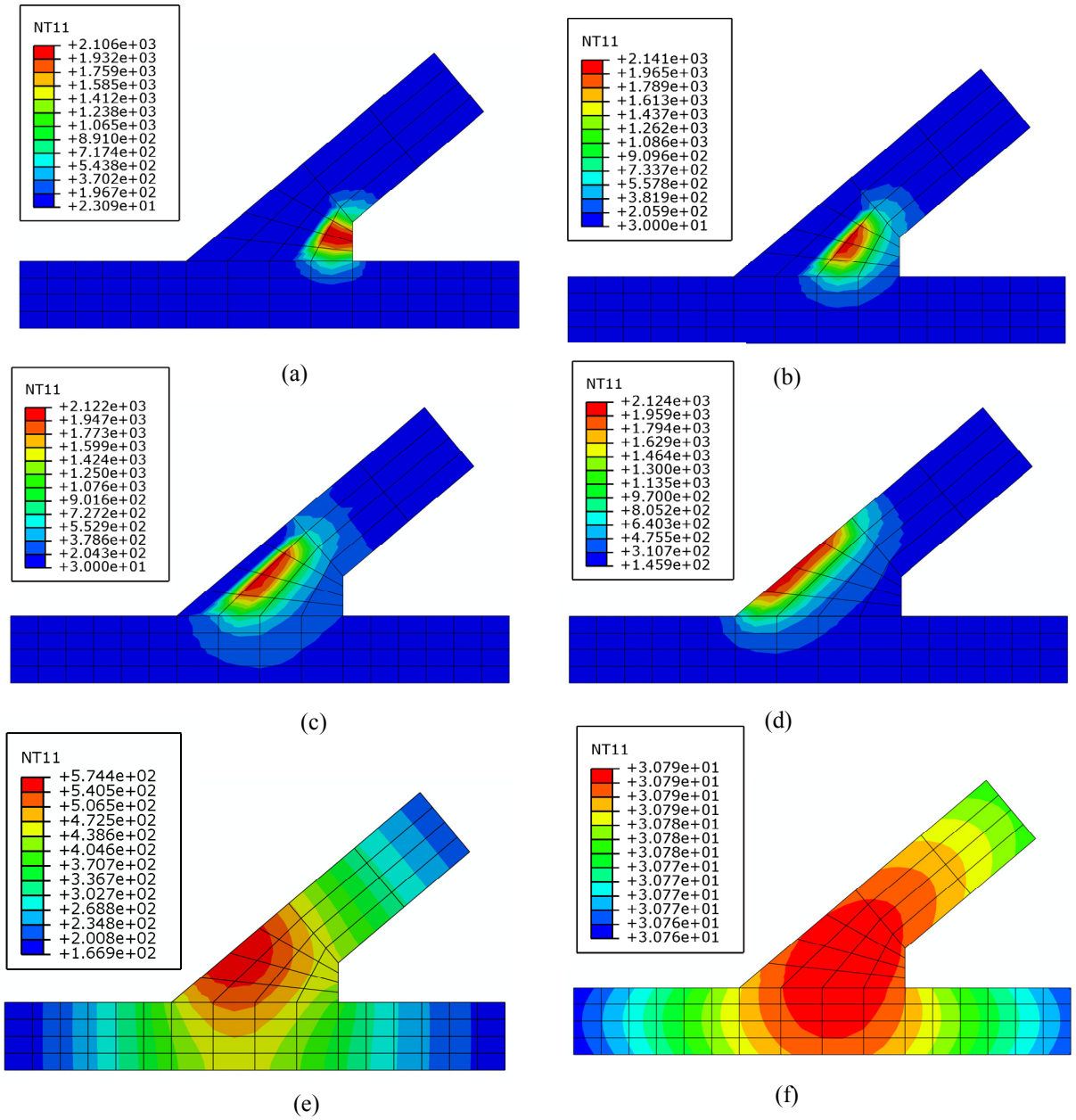

Fig. 9 Temperature distributions at different times
(θ=135°, t_1=12mm, welded at ambient temperature)
(a) t=1.0s, (b) t=58.7s, (c) t=117.4s, (d) t=176.1s, (e) t=300s, (f) t=2500s

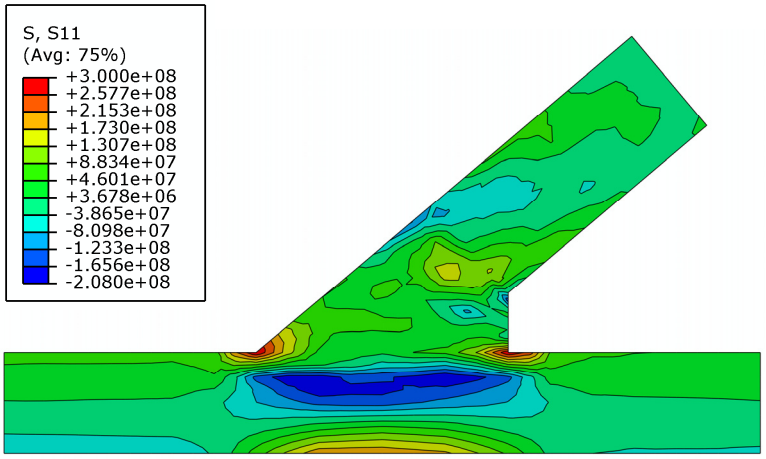

(a) 100°C preheating

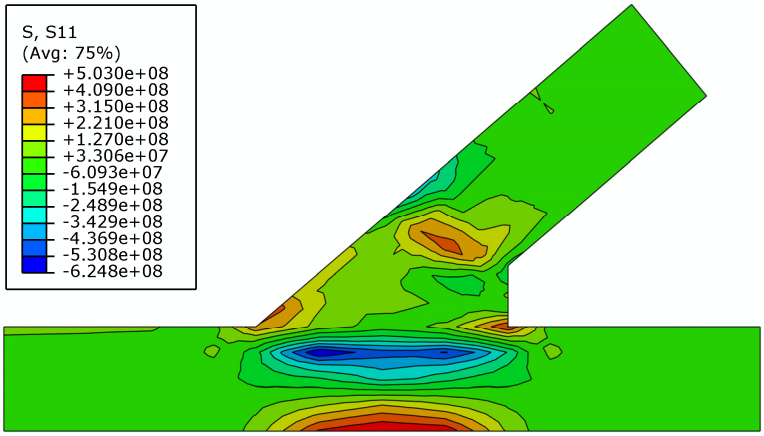

(b) Ambient temperature

Fig. 10 The final residual stress distribution (θ=135°, t_1=12mm)

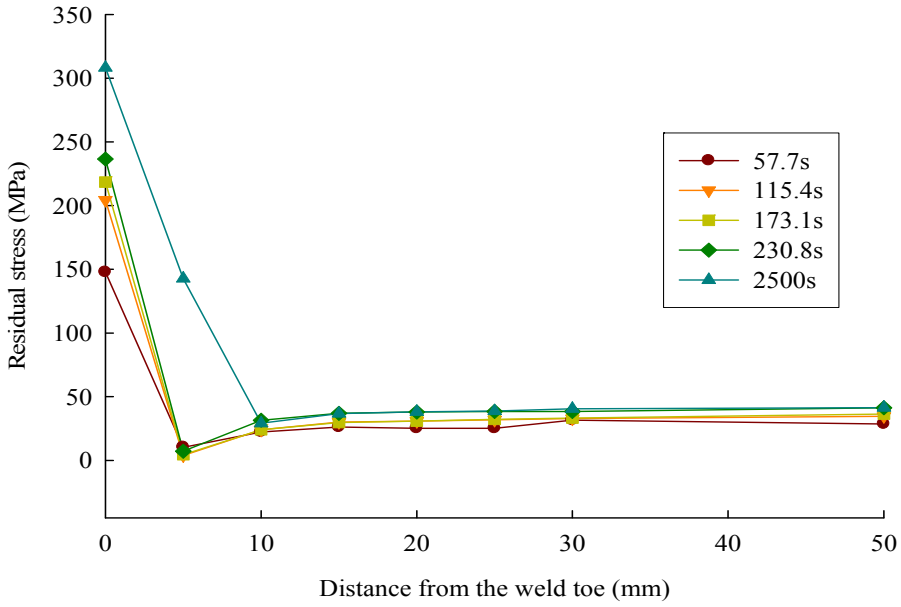

Fig. 11 Development of transverse residual stress for joint with preheating (θ=135°, t_1=12mm)

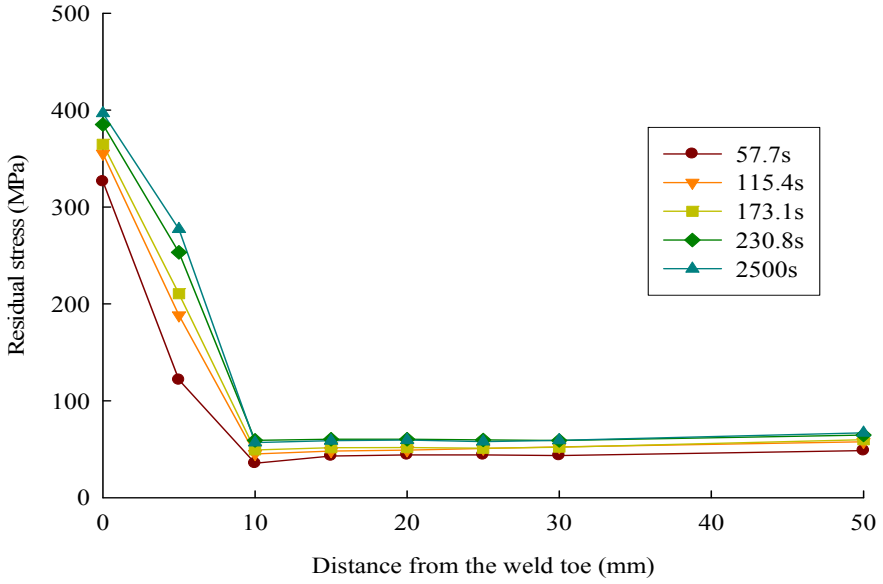

Fig. 12 Development of transverse residual stress for joint welded at ambient temperature (θ=135°, t_1=12mm)

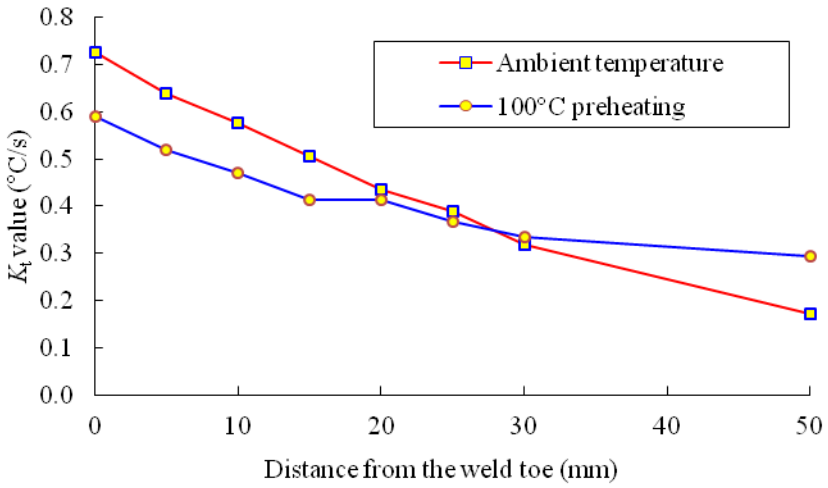

Fig. 13 Average cooling rates for joints with and without preheating (θ=135°, t_1=12mm)

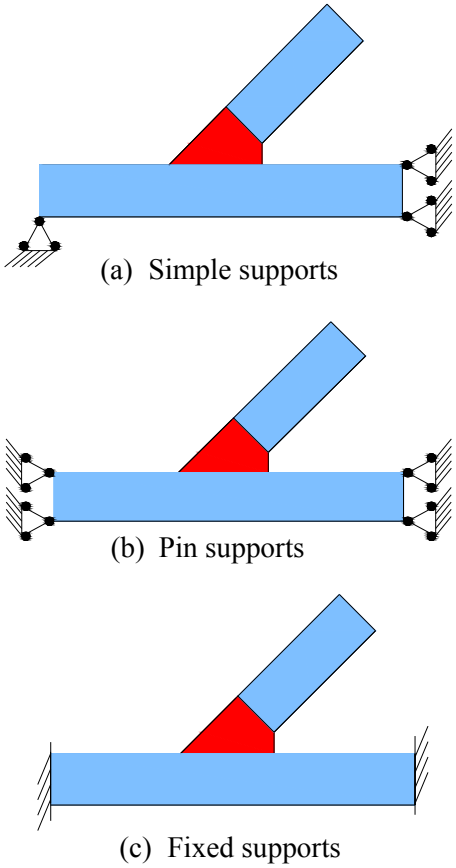

Fig. 14 Different boundary conditions employed in the parametric study

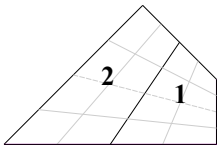

2 lumps

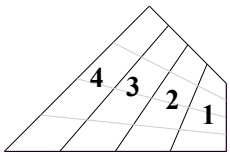

4 lumps

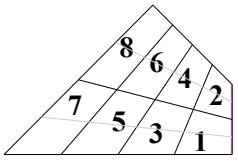

8 lumps

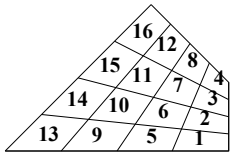

16 lumps

Fig. 15 Different lumping schemes employed in the parametric study

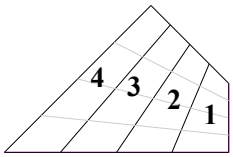

Case: a

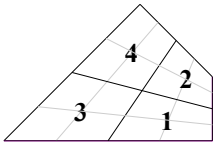

Case: b

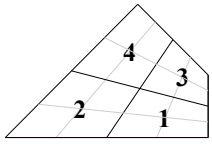

Case: c

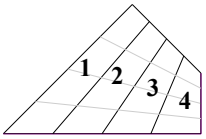

Case: d

Fig. 16 Different weld sequences employed in the parametric study

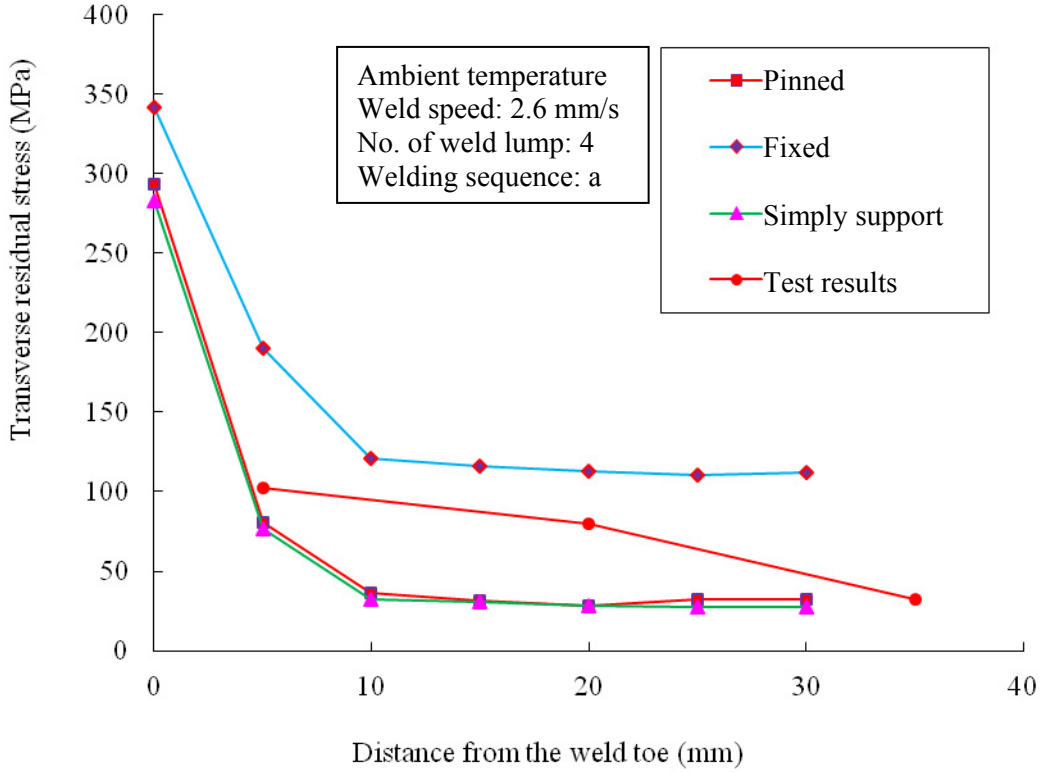

Fig. 17 Comparison of transverse residual stress under different boundary conditions

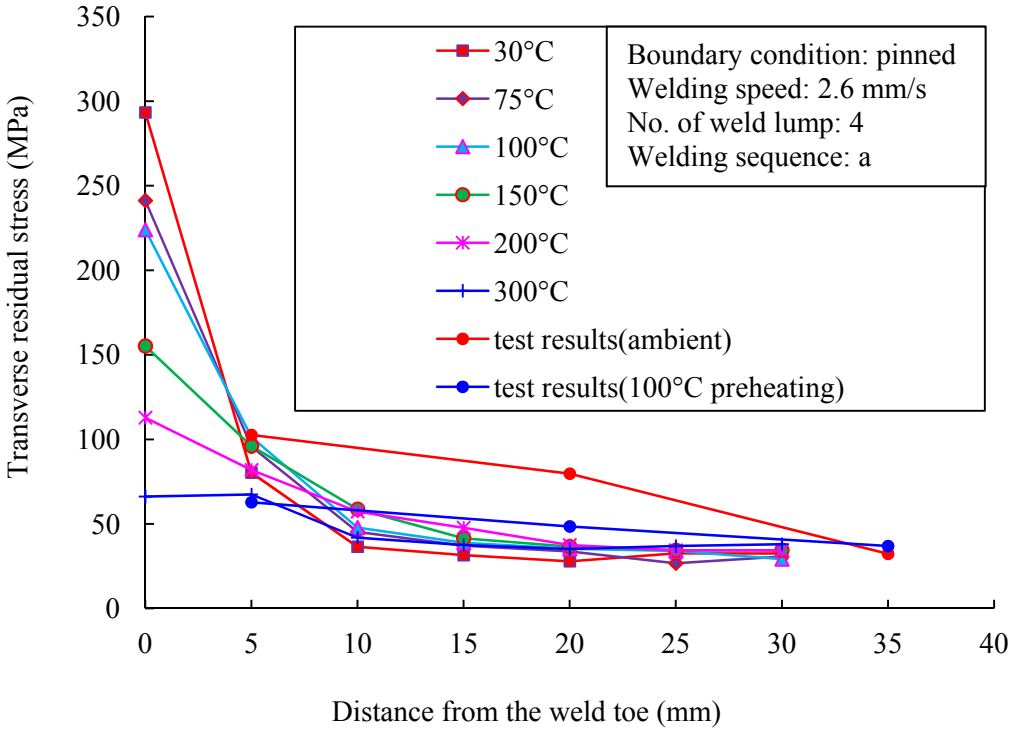

Fig. 18 Comparison of transverse residual stress for different preheating temperatures

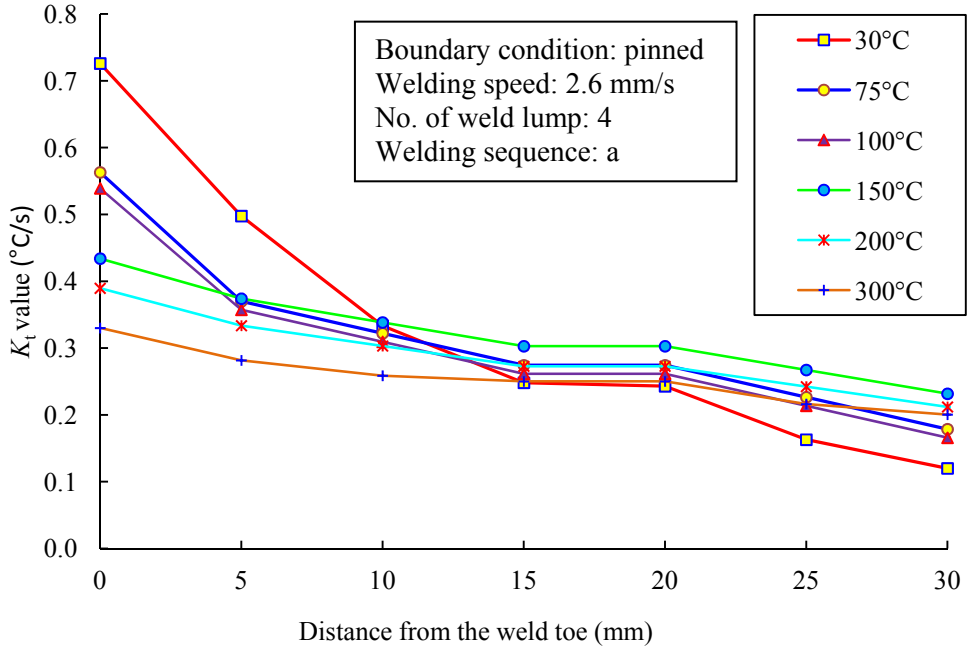

Fig. 19 Average cooling rates for different preheating temperatures

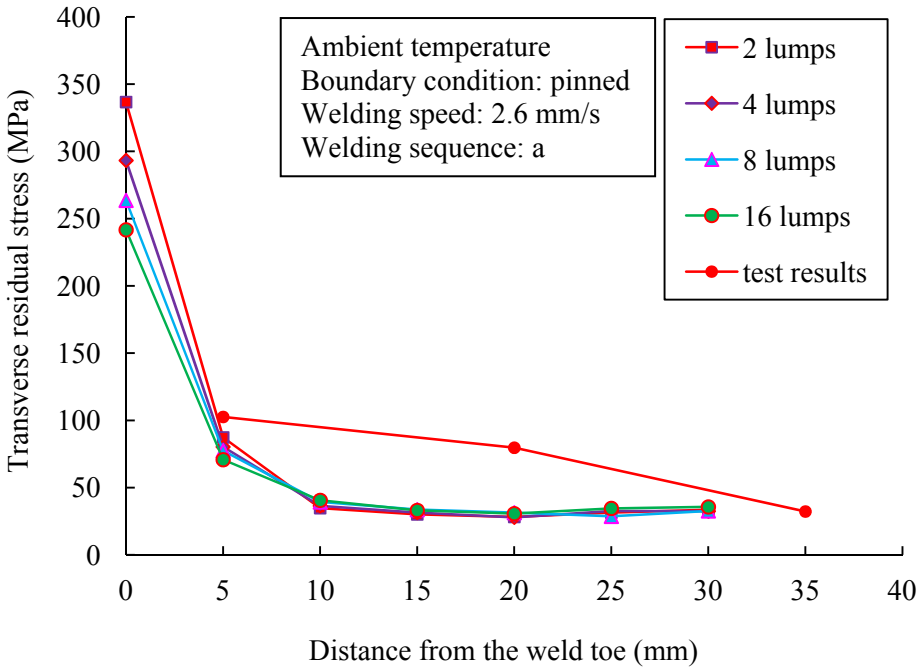

Fig. 20 Comparison of transverse residual stress for different weld lumping schemes

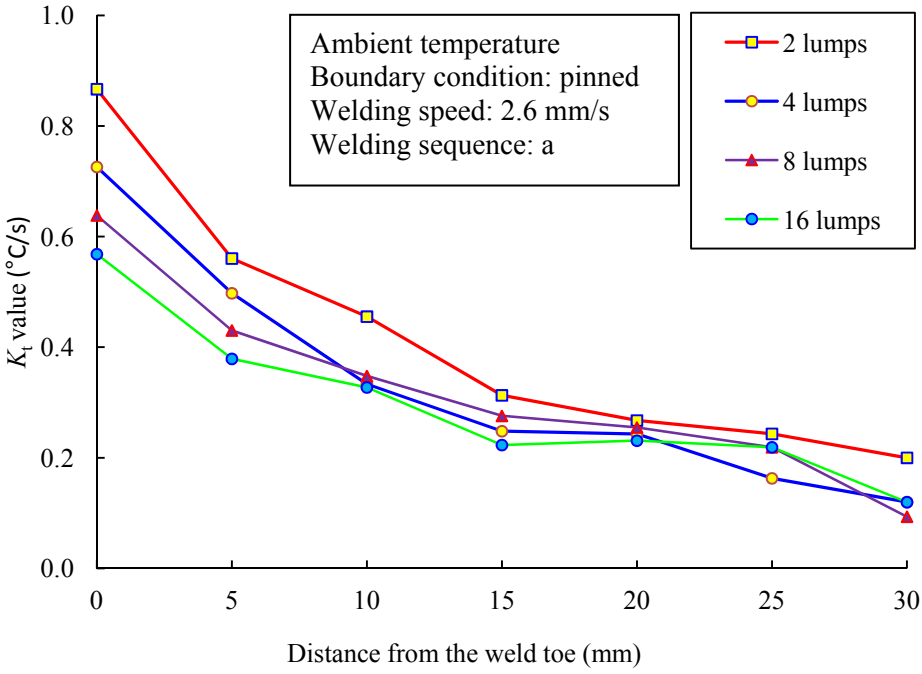

Fig. 21 Average cooling rates for different lumping schemes

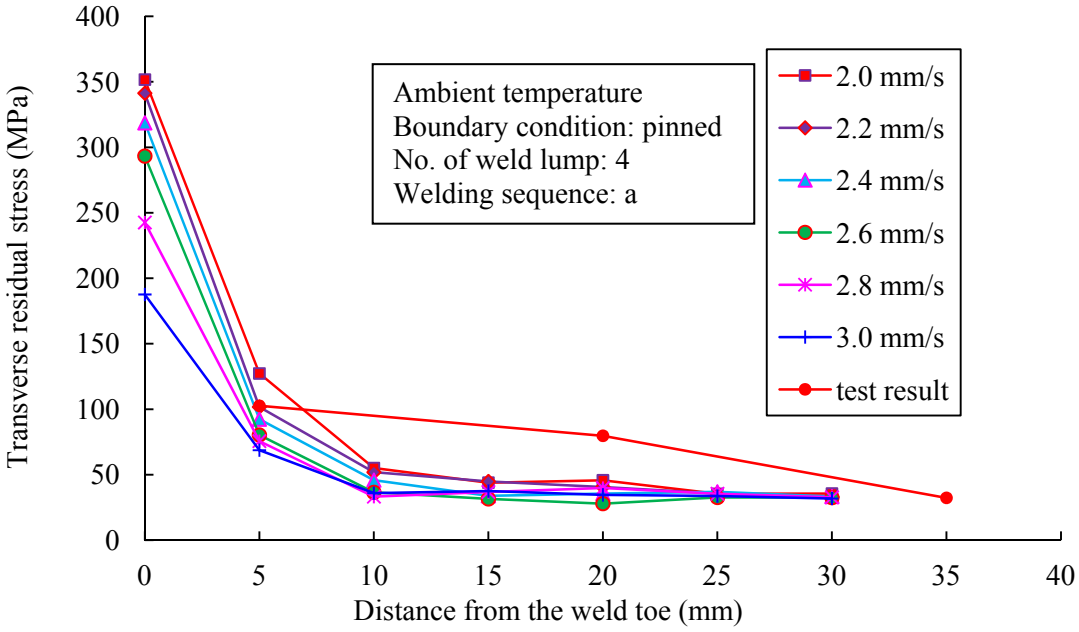

Fig. 22 Comparison of transverse residual stress for different welding speeds

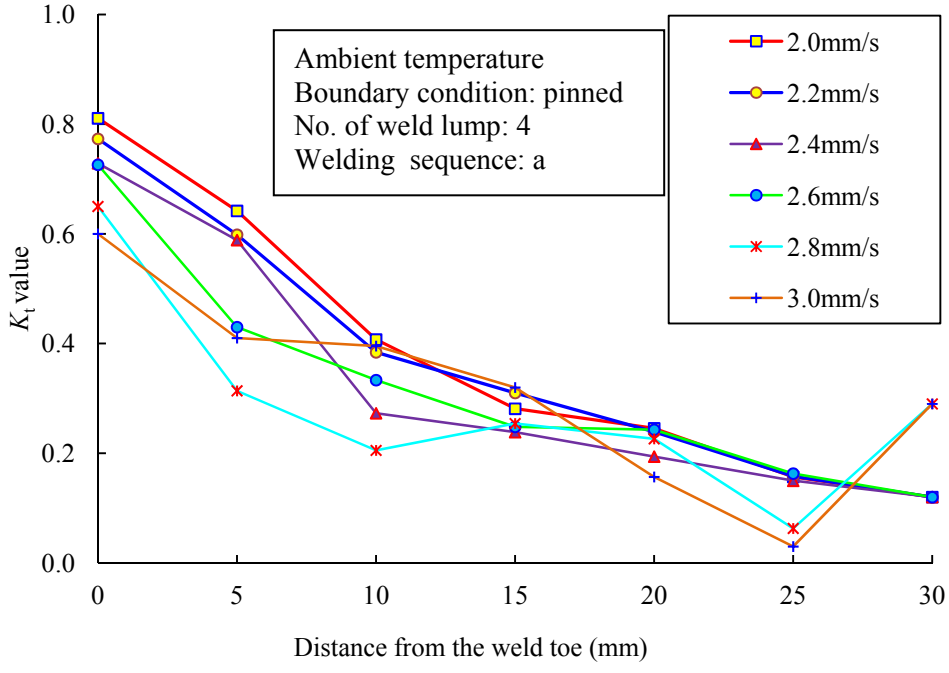

Fig. 23 Average cooling rates for different welding speeds

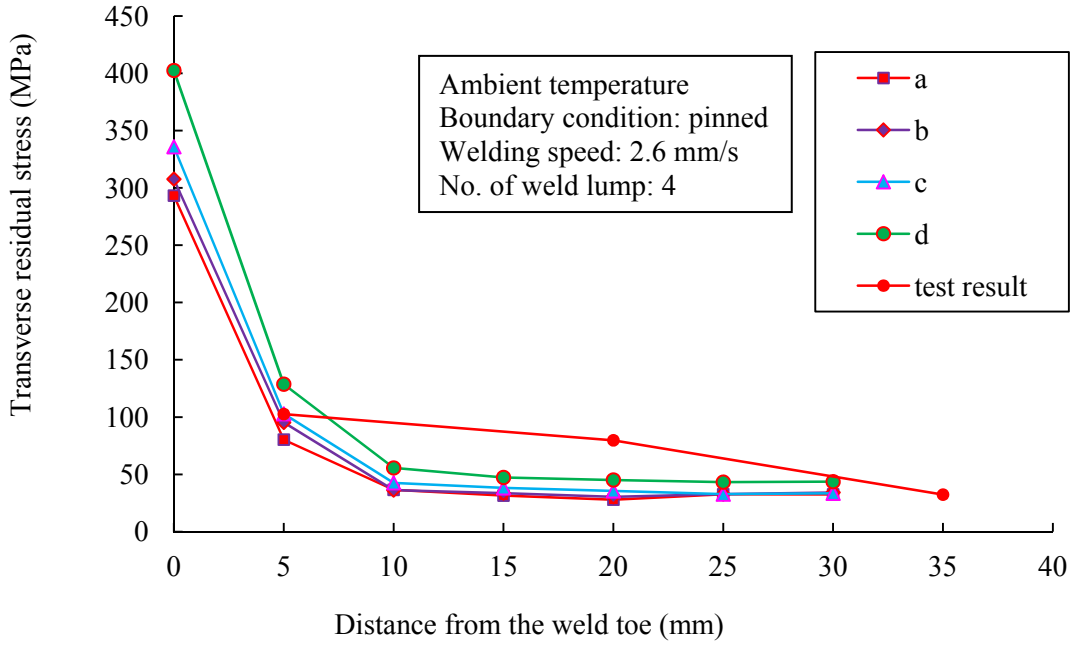

Fig. 24 Comparison of transverse residual stress for different welding sequences

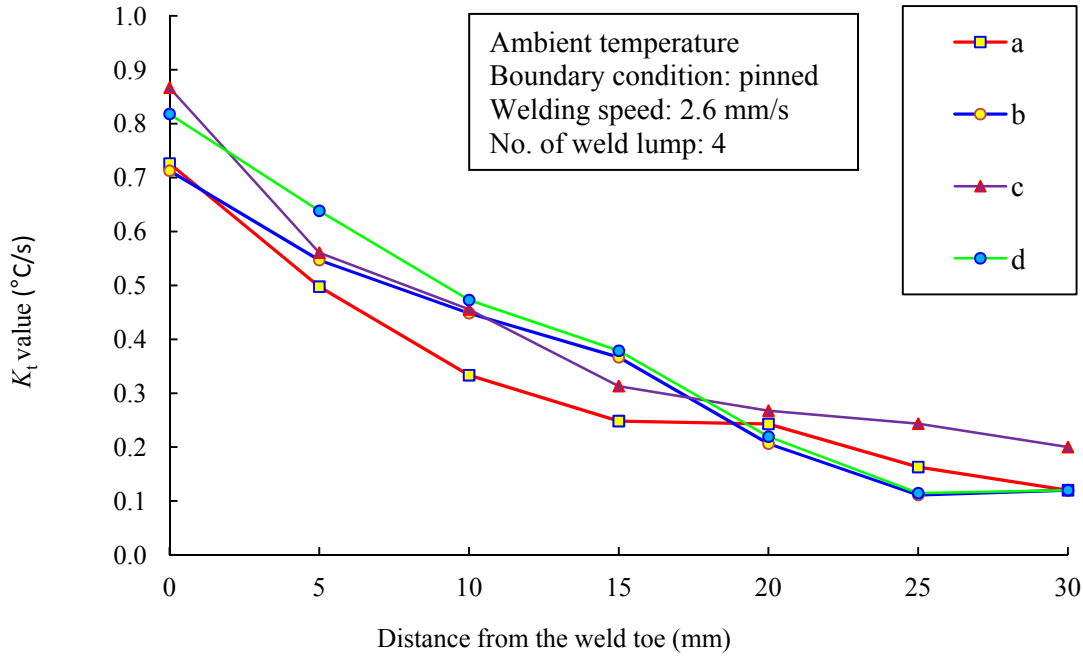

Fig. 25 Average cooling rates for different welding sequences

Table 1 Summary of the sequentially-coupled thermal-stress analysis procedure

Analysis / modeling elements	Heat Transfer	Stress Analysis
Element type	Four-node, linear-interpolation, heat- transfer element: DC2D4	Four-node bilinear plane strain quadrilateral, reduced integration element: CPE8R
Boundary conditions and loading	Surface film Surface radiation	Temperature 'load' via ODB file
Material Properties	Specific heat Density Conductivity	Elasticity Plasticity Thermal expansion
Numerical formulation	Transient thermal analysis	Elastic-plastic analysis

Table 2 Modeling results at selected points
(For exact positions of points B, B1, B2, B3, see Fig. 7 of reference [25])

Specimen			Residual stress computed at measuring points (MPa)						
θ (°)	t (mm)	Preheating	Weld toe	5mm (point B)	10mm	15mm	20mm (point B1)	35mm (point B2)	50mm (point B3)
90	8	Yes	96.7	69.2	42.3	41.1	40.5	40.1	21.7
		No	154.2	88.6	67.3	40.2	39.7	38.2	15.4
	12	Yes	167.8	98.4	77.3	42.1	40.3	39.6	5.7
		No	194.7	105.3	74.5	32.8	32.4	31.6	9.7
	16	Yes	197.8	97.3	81.5	41.1	40.8	40.3	12.7
		No	225.4	106.7	87.6	37.4	37.1	36.5	15.8
135	8	Yes	211.1	102.4	74.3	44.9	44.1	43.6	14.9
		No	254.6	126.7	65.4	42.8	42.2	41.7	17.6
	12	Yes	224.1	101.4	47.8	38.8	35.3	34	21.7
		No	293.3	86.3	36.5	31.5	27.9	32.6	22.9
	16	Yes	234.1	121.7	54.3	51.3	50.7	50.1	25.7
		No	278.5	149.4	57.9	53.4	52.7	52.3	23.1

Table 3 Summary of the models employed in the parametric study
Joint dimension: θ=135, t_1=12mm
(For exact positions of points B and B1, see Fig. 7 of reference [25])

Cases			Residual stress computed at selected points						
Parameter considered		Other modeling conditions	0mm (weld toe)	5mm (Point B)	10mm	15mm	20mm (Point B1)	25mm	30mm
Boundary conditions	Fixed	Ambient temperature Welding speed: 2.6 mm/s No. of lump: 4 Welding sequence: a	293.3	80.3	36.5	31.5	27.9	32.6	32.5
	Pinned		341.9	190	120.6	115.7	112.6	110.7	112.3
	Simply support		282.6	76.8	32.1	30.5	28.4	27.6	27.4
Preheating temperature	30°C	Boundary condition: pinned Welding speed: 2.6 mm/s No. of lump: 4 Welding sequence: a	293.3	80.3	36.5	31.5	27.9	32.6	32.5
	75°C		241.2	95.7	45.3	37.1	33.7	26.7	30.7
	100°C		224	101.4	47.8	38.8	35.3	34	29.2
	150°C		155.2	96.1	58.7	41.5	36.6	34.4	34.5
	200°C		112.8	81.9	57.3	47.7	37.5	34.4	34.3
	300°C		66.2	67.4	41.9	37.5	35.1	36.9	38.0
Numbers of lumps	2	Ambient temperature Pinned support Welding speed: 2.6 mm/s Welding sequence: a	336.7	87.4	34.8	30.1	28.2	31.4	33.6
	4		293.3	80.3	36.5	31.5	27.9	32.6	32.5
	8		263.6	77.5	39.4	33.7	31.4	28.7	32.7
	16		241.7	70.8	40.6	33.1	30.7	34.6	35.7
Welding speed	2.0mm/s	Ambient temperature Pinned support No. of lump: 4 Welding sequence: a	**351.7**	**127.3**	**55.1**	**43.9**	**45.7**	**35.4**	**35.6**
	2.2 mm/s		**341.3**	**101.7**	**51.9**	**44.8**	**40.6**	**35.7**	**32.9**
	2.4 mm/s		**318.7**	**92.4**	**45.8**	**33.8**	**35.6**	**36.9**	**33.4**
	2.6 mm/s		293.3	80.3	36.5	31.5	27.9	32.6	32.5
	2.8 mm/s		**242.6**	**75.6**	**33.2**	**36.8**	**39.8**	**35.4**	**32.7**
	3.0 mm/s		**187.6**	**68.7**	**35.9**	**37.5**	**34.6**	**33.7**	**31.8**
Welding sequence	a	Ambient temperature Pinned support Welding speed: 2.6 mm/s No. of lump: 4	293.3	80.3	36.5	31.5	27.9	32.6	32.5
	b		307.7	95.3	36.2	33.6	30.4	32.7	34.2
	c		335.9	102.8	42.6	38.2	35.6	32.7	33.5
	d		402.5	128.7	55.6	47.3	45.1	43.2	43.6